

Article

A Comprehensive Analysis of the Penetration of Detailed Type 4 Wind Turbine Generators in the Two-Area Benchmark System

Rodrigo Trentini ^{1,*}, Rüdiger Kutzner ², John J. A. Saldanha ^{1,3}, Ademir Nied ^{3,*},
Tiago Jackson May Dezuo ³ and Mariana Santos Matos Cavalca ³

¹ Department of Electrical Engineering, Federal Institute of Santa Catarina—IFSC, R. dos Imigrantes 445, Jaraguá do Sul 89254-430, Brazil; john.saldanha@ifsc.edu.br

² Department of Control Engineering and Mechatronics, University of Applied Sciences and Arts Hannover—HsH, Ricklinger Stadtweg, 30459 Hannover, Germany; ruediger.kutzner@hs-hannover.de

³ Department of Electrical Engineering, Santa Catarina State University—UDESC, R. Paulo Malschitzki 200, Joinville 89219-710, Brazil; tiago.dezuo@udesc.br (T.J.M.D.); mariana.cavalca@udesc.br (M.S.M.C.)

* Correspondence: rodrigo.trentini@ifsc.edu.br (R.T.); ademir.nied@udesc.br (A.N.)

Abstract: The shift towards RES introduces challenges related to power system stability due to the characteristics of inverter-based resources (IBRs) and the intermittent nature of renewable resources. This paper addresses these challenges by conducting comprehensive time and frequency simulations on the IEEE two-area benchmark power system with detailed type 4 wind turbine generators (WTGs), including turbines, generators, converters, filters, and controllers. The simulations analyse small-signal and transient stability, considering variations in active and reactive power, short-circuit events, and wind variations. Metrics such as rate of change of frequency (RoCoF), frequency nadir, percentage of frequency variation, and probability density function (PDF) are used to evaluate the system performance. The findings emphasise the importance of including detailed models of RES in stability analyses and demonstrate the impact of RES penetration on power system dynamics. This study contributes to a deeper understanding of RES integration challenges and provides insights for ensuring the reliable and secure operation of power systems in the presence of high levels of RES penetration.

Keywords: renewable energy sources; wind turbine generator; penetration of RES; two-area benchmark system; inverter-based resources



Citation: Trentini, R.; Kutzner, R.; Saldanha, J.J.A.; Nied, A.; Dezuo, T.J.M.; Cavalca, M.S.M. A Comprehensive Analysis of the Penetration of Detailed Type 4 Wind Turbine Generators in the Two-Area Benchmark System. *Energies* **2023**, *16*, 4970. <https://doi.org/10.3390/en16134970>

Academic Editors: Davide Astolfi, Mohit Bajaj, Padmanabh Thakur, Olena Rubanenko and Arvind R. Singh

Received: 17 May 2023
Revised: 16 June 2023
Accepted: 22 June 2023
Published: 27 June 2023



Copyright: © 2023 by the authors. Licensee MDPI, Basel, Switzerland. This article is an open access article distributed under the terms and conditions of the Creative Commons Attribution (CC BY) license (<https://creativecommons.org/licenses/by/4.0/>).

1. Introduction

The world is shifting towards renewable energy sources, such as hydro, biomass, wind, and solar PV, to reduce reliance on traditional thermal sources, such as coal and gas. This transition aligns with the Paris Agreement's goal of limiting global temperature rise. Over 130 countries have committed to the Net Zero Emissions by 2050 Scenario, reflecting the importance of sustainable energy and combating climate change. The International Energy Agency (IEA) tracks the growth of renewables and reports a rise in power generation from RES, increasing from 19.8% to 28.7% between 2010 and 2021 [1]. However, more progress is needed to meet the targets, requiring the renewable share of power generation to surpass 60% by 2030. Wind power is a leading non-hydro technology, with significant growth in 2021, led by China, the United States, and Brazil [2].

All of these data highlight the importance of continuous evolution of RES technology, which is not only vital for improving the performance and reliability of current systems but also for driving down costs and making renewable energy more competitive with traditional energy sources. Additionally, emerging technologies, such as energy storage, smart grids, and carbon capture and storage, can further enhance the capabilities and flexibility of renewable energy systems.

On the other hand, compared to all the cited development and sharp increase in RES share, researchers and practitioners have detected some issues concerning high levels of penetration of this type of energy in actual power systems. For instance, the use of power converters imposes new challenges for the integration of power systems, such as low inertia, low short-circuit capability, high nonlinearities, and resource intermittency. The atypical response to a power outage at the Hornsea offshore wind farm—which caused a blackout in the UK grid in August 2019—provides compelling evidence of the need for caution when increasing RES penetration in power systems. Some previous works on RES penetration often assumed that synchronous generators could compensate for frequency fluctuations, which is generally true for large power systems with sufficient reserves. However, this assumption does not hold for small systems or islanded grids. As large-scale thermal power plants are replaced by RES, the frequency of the power system present accentuated variations, and power quality may be significantly affected. These fluctuations may result in frequent load shedding and, in severe cases, even blackouts [3].

According to Shair et al. [4], compared to traditional synchronous generators (SGs), the inertia of inverter-based resources (IBRs) of grid following type is significantly lower. This is because the power electronic converter interface separates the input power of the prime mover from the output electromagnetic power of the grid, resulting in a lack of traditional inertia response based on rotational kinetic energy. Furthermore, the energy storage elements in IBRs, such as inductors and capacitors, have limited ability to absorb and discharge power deviations caused by disturbances and resist frequency deviations on the grid [5,6].

However, power electronic equipment has a smaller short-circuit current capacity compared to SGs. Power electronic equipment does not have a sub-transient process during a short-circuit fault. Although the initial short-circuit current is low, the steady state short-circuit current decreases rapidly because of its high internal reactance and fast controllable reference current. Consequently, the amplitude and time span of the short-circuit current are smaller than those of traditional SGs, which presents challenges in controlling and protecting power electronic equipment [7].

Wu et al. [8] and Shah et al. [9] state that, compared to traditional SGs, IBRs exhibit more pronounced nonlinear characteristics due to various factors. These include discrete switching operations, control nonlinearities, such as limiters and saturation triggered by overloading, and sequential switching of control and protection strategies under different modes, such as P/Q and V/f, as well as operating conditions. According to Mansour et al. [10], although IBRs are efficient in converting power, they encounter challenges in maintaining stability when connected to weaker grids and may experience synchronisation issues with the grid.

At last, perhaps the most known issue faced by RES is unpredictability. The power output of IBRs is dependent on variable environmental and climatic factors, such as wind speed and solar irradiance, which can change continuously. In contrast, SGs have controllable primary sources, such as coal and water, which are stable and predictable. Although the wind and solar powers can be forecasted, there are significant uncertainties associated with these predictions [11].

The stability of a power system can be basically assessed in two perspectives: small- and large-signal stability. Small-signal stability analysis assesses the ability of the power system to remain synchronised with the grid despite small disturbances. Mansour et al. [10] investigate the small-signal stability analysis in power systems with RES from the injected current on the point of common coupling (PCC). This injection affects the phase-locked loop (PLL), creating a positive feedback loop called a “self-synchronisation loop”, which can lead to system instability, especially if a high-gain PLL is used. Furthermore, synchronisation instability can generate sideband oscillations in voltage and current waveforms. Large-signal or transient stability analysis, in contrast, examines the existence of an equilibrium point for the system under normal and faulty conditions. This type of instability can occur if the system lacks a stable equilibrium point or does not have sufficient damping to drive the

system towards the equilibrium point. In transient stability analysis of power systems with RES, the converter is considered an ideal controllable current source as the PLL dynamics are much slower than the inner control loops.

Several researchers (e.g., [12–20]) observed that the increase in RES poses various challenges to the stability of power systems. The physical structure, mechanical characteristics, energy conversion mechanism, and control characteristics of power generators and equipment have a significant impact on the stability characteristics of traditional power systems based on SGs. As the proportion of renewable energy and power electronic converter equipment increases, the impact of it depends largely on the location in the system. The extent of the influence on system stability is determined by the share of renewable energy and power electronic equipment. Therefore, it is essential to consider the impact of renewable energy and power electronic equipment on system stability and coordinate their dynamics to ensure reliable and secure operation of power systems.

Hence, the use of reliable simulation models is crucial in accurately evaluating the effects of high penetration of RES on power systems. It is imperative to thoroughly investigate the impacts of renewables on known power systems to compare the potential effects in a more realistic way. Trøndheim et al. [21] show interesting results on the stability of the Suðuroy (Faroe Islands) grid. The findings suggest that the use of approximated models for frequency and voltage regulation, which exclude inverter-based resources, is insufficient. These sources must be included in the approximation through triggered behaviours or the use of detailed models. This conclusion is applicable not only to the Faroese power system or isolated power systems but to all power systems that utilise frequency-triggered technologies and simplify simulations to reduce computational time. The authors also suggest that it is crucial to examine the system gradually, considering not only the initial and final states (e.g., current and far future condition) but also intermediate stages as expansions in between could potentially cause instabilities, even if the final system configuration does not exhibit any issues. Taul et al. [22] also exemplify that, when grid-tied converters are exposed to severe grid faults, they can suffer from transient instability and synchronisation loss. As these phenomena involve large-signal disturbances, a linearized equivalent of the system may no longer provide accurate results. To address this issue, a widely used approach is to perform time-domain simulation studies using a detailed model of the system. Despite an eventual computational burden, it allows for a comprehensive assessment of the system transient stability and overall performance.

However, simplified models are often utilised for analysis and controller design purposes. For instance, Gayathri et al. [23] conducted several simulations to investigate the impact of high RES penetration on power system dynamics using both IEEE-9 bus system and the two-area system with simplified wind turbine generators (WTGs) models. Various common contingencies, such as generation outage, generation reduction, load shedding, and three-phase faults, were considered in the analysis, where one of the SGs of each system is replaced by a WTG. The penetration percentage of RES is changed with the increase in generated power of the single simplified WTG. The results show that the replacement of conventional sources with RES can cause a steep frequency plot, leading to a significant reduction in frequency nadir. The study highlights the need for careful consideration of RES integration in power systems and the importance of addressing the impact on system dynamics, although without analysing detailed WTG integration. Wilches-Bernal et al. [24] investigate the impact of wind integration on the inter-area oscillation using a simple two-machine two-area system. The WTGs use average models for the converters and the penetration of RES is tested from 0% to 43%. The results demonstrate that, while wind integration can increase the damping of the interarea mode, it has the potential to destabilise the system when WTGs are installed in the area that imports power. Similarly, Piccoli et al. [25] use the four-machine two-area system with linearized models for the converters to investigate the impact of the penetration of RES in an islanded power system. Four scenarios (0%, 25%, 50%, and 75%) of RES penetrations are tested. The paper concludes that the behaviour of the power system becomes unstable for load

and generator input power variations when two or more WTGs replace the original SGs and exhibits oscillatory behaviour during a three-phase fault. According to the authors, this instability raises concerns about the increasing penetration of RES in power systems, it being, therefore, necessary to conduct in-depth studies on effective control methods to mitigate such problems. In [26], the authors use an artificial neuro-fuzzy inference system (ANFIS) to map measurements from phasor measurement units (PMUs) to the external equivalent model of the Northeast Power Coordinating Council (NPCC) power system, treating it as a black box. This approach has been extensively used in the literature and has the benefit of not requiring a mathematical model of the system or extensive computational simulations. However, it does not provide detailed information on the signals of each machine, control saturation, limiting the ability to understand the effects of various scenarios, particularly when RES are integrated. Dong et al. [27] examine the correlation between small-signal stability and grid strength as measured by the short circuit ratio (SCR) in a single-infeed power electronic system using analytical techniques to extend these relationships to a multi-infeed power electronic system (MIPES) through eigenvalue decomposition. The aim is to provide a thorough mathematical explanation for stability assessment of power converters with reduced computational burden. However, the converters are not modelled in detail, and machine dynamics are not considered, which limits the ability to understand the impact of integrating renewable energy sources (RES) in large-scale power systems. An interesting work on a simplified model of a type 3 WTG is presented in [28], which incorporates an approximate representation of the power electronic converter. The primary objective of the model is to reduce computational effort while analysing the dynamics of instantaneous electrical variables. This allows for an expansion in the scope of network studies related to primary frequency control and power quality studies in high-penetrated wind power systems, all at a lower cost and computational time. The results of the study demonstrate a minimal delay between the proposed model. The authors claim that transient and steady state responses are accurately approximated by the simplified model; however, neither is a short-circuit simulation conducted—which is known as the worst case for transient stability analysis—nor an extended power system tested. Other examples of usage of simplified models can be found, such as [29–33].

Therefore, the objective of this study is to make a significant contribution to the existing literature by conducting a comprehensive investigation on the penetration of detailed WTGs of type 4 using time and frequency simulations, including their turbines, generators, switching converters, filters, and associated controllers. To accomplish this, the research employs the widely recognised two-area system, initially introduced by [34], as the benchmark for the analysis. This system is chosen due to its extensive use in power system stability analysis, thereby ensuring that the reference outcomes (with four SGs) are widely documented in previous studies (e.g., [35,36]). The ultimate goal of this paper is to provide a more profound understanding of the effects of RES penetration on power systems that experience high power transfer between distinct regions. By the end of this study, we aim to shed light on the intricate dynamics of power systems under these conditions, thus contributing significantly to the existing knowledge in this area.

To that aim, the paper provides a detailed overview of the study power system, including information on machines, turbines, converters, and controllers in Section 2. The obtained simulated results are presented in Section 3, which includes time and frequency simulations for both small-signal and transient stability analysis. The simulations test changes in active and reactive power reference, short-circuit events, and variations in wind, with the results analysed using metrics such as rate of change of frequency (RoCof), frequency nadir, and probability density function (PDF). Section 4 presents discussions on the results, the main contributions of the work, and final conclusions.

2. Materials and Methods

The present work focuses on analysing the original two-area benchmark system, commonly referred to as Kundur's system, as mentioned in the Introduction. Figure 1

illustrates the system, which consists of four SGs rated at 900 MVA/20 kV, with generator 2 acting as the swing bus. The system is symmetrical and is divided into two areas, namely area 1 and area 2, each having two groups of generators. These two areas are connected by two long 230 kV transmission lines in parallel, each spanning 220 km. The loads are located at the end of each area, with the active power of the load in area 2 being nearly twice that of area 1, resulting in a power transfer of approximately 420 MW from area 1 to area 2. Generators 1 and 4 provide 700 MW each, whilst generator 3 provides 719 MW and generator 2 the remaining 795 MW to maintain grid stability.

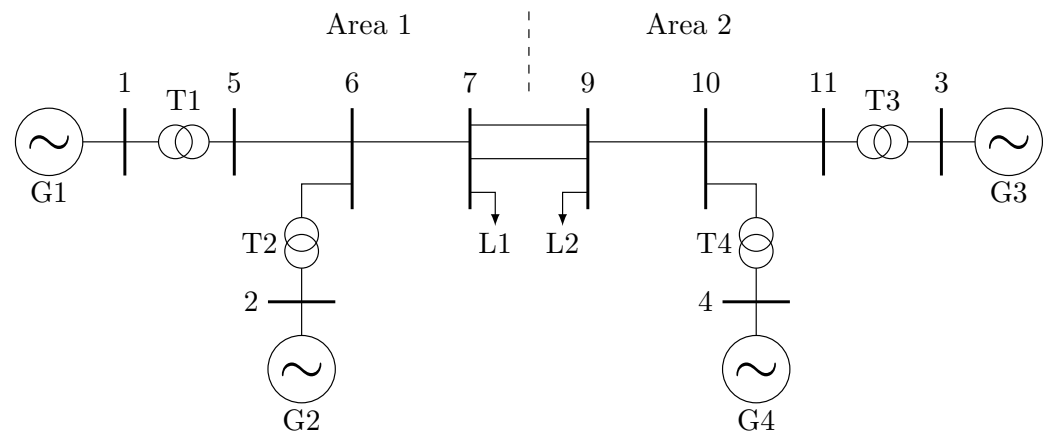


Figure 1. Four-machine two-area benchmark system.

All prime movers are of the thermal type (steam turbine), and the governors utilise droop control. The excitation system comprises an automatic voltage regulator (AVR) and power system stabiliser (PSS). It is important to note that, without the PSSs, the two-area system would be inherently unstable. Further details about the system are presented in [37]. All simulations run in Matlab[®]/Simulink[®] with the toolbox Simscape Electrical[™].

The schematic of the WTGs that replaces the original SGs is shown in Figure 2. The WTGs have equivalent rated power and consist of a wind turbine, SG, rectifier, boost converter, inverter, and filter. The system includes controllers for pitch angle, active and reactive power, DC-link, and field voltages, which are discussed in detail in the next section.

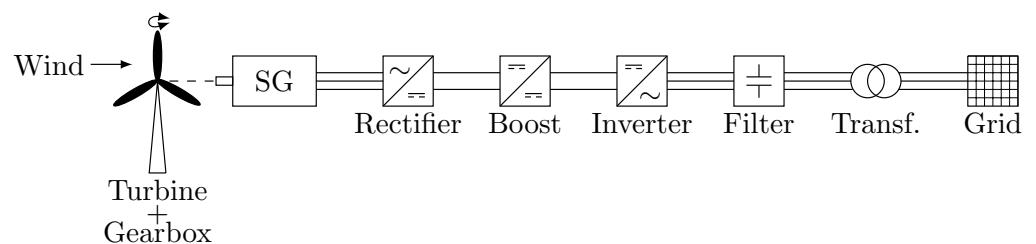


Figure 2. Type 4 wind turbine generator.

2.1. Detailed Type 4 WTG

The wind turbine model is based on [38], whilst the SG with field winding is obtained directly from the block diagram of the Matlab[®]/Simulink[®] Simscape Electrical[™] toolbox. Rectifier, boost converter, and inverter are regarded with their switching behaviour. This fact increases the computation time, but it delivers a higher amount of reliability to the simulations.

The implemented WTG mimics a wind farm composed of 450 WTGs of 2 MVA each, given that the implementation of such amount of WTGs in a simulation environment is impractical due to the computational burden. It means that all aspects of the WTG must be converted to rated power, including generator reactances, time and inertia constants, snubber resistances and capacitances, switches/diodes forward resistances, boost and filter inductances, resistances, and capacitances. All amounts are regarded in pu. The original data for the 2 MVA WTG are obtained from [39].

It is important to highlight that elements that are commonly implemented with WTGs for stability improvements—such as grounding transformers, synchronous converters, etc.—are not present in the proposed implementation since the main idea of this work is exactly to experiment the replacement of SGs with WTGs to verify system stability without any other countermeasure.

Moreover, some highly cited papers in the RES literature, such as Ratnam et al. [5], Saha et al. [11], Alam et al. [12], Tróndheim et al. [21], cite that the gearbox does not impose important issues in load flow and dynamic behaviour of the power system. Therefore, this item is not considered in the simulations of this work.

As previously cited, each WTG has five PI-based control loops implemented with saturation and anti-wind-up effect: one for active power, one for reactive power, one for the pitch angle, one for the DC-link voltage, and one for the field voltage. Next sections detail each of them.

2.1.1. Active Power Controller

Notice that, differently from other studies where the WTG injects power into the grid according to its generation, this work uses an active power control loop to establish a constant injected power regardless of the generation—provided that the generation is equal or higher than the active power setpoint.

In fact, the active power controller has a cascade structure as shown in Figure 3, with P_r and i_r being the references for active power and inductor current, and P_m and i_L being the measured corresponding signals. The outer loop controls the active power, whilst the inner one regulates the boost converter inductor current. The current controller provides the duty cycle percentage used for a 2 kHz PWM generation for the boost switch.

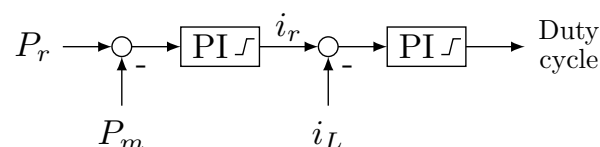


Figure 3. Active power control structure.

2.1.2. Pitch Angle Controller

The pitch angle controller is composed of a single loop and is based on the reference shaft speed ($\omega_r = 1$ pu). A rate limiter is used given that the variation in the pitch angle is relatively slow due to its dynamics. Figure 4 shows the block diagram for its control loop, with ω_m being the measured shaft speed.

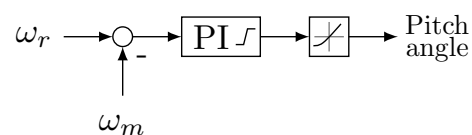


Figure 4. Pitch angle control structure.

2.1.3. Field Voltage Controller

The traditional SGs terminal voltage signal is not suitable for WTG feedback of type 4. For this kind of machine, a flux estimator is required. In this work, the quasi-steady-state flux estimator presented by Trevisan et al. [39] is used. The estimated flux is then fed back to the control loop. Its reference may vary depending upon the machine speed. If it is lower than 1 pu, the flux reference is set to 1 pu. On the other hand, if the machine speed is greater than 1 pu, then the reference flux is given by the inverse of the same speed. The error between the reference and estimated fluxes is computed by a PI controller, which provides the necessary field voltage that ensures the required electromagnetic torque of the machine. Figure 5 exemplifies the cited control loop.

8. 72% of RES—G1, G3, and G4 are replaced by WTGs of the same rated powers.

Given that this work aims to provide a comprehensive analysis for each cited case, the following simulations are proposed:

1. Short-circuit (transient analysis)—a 200 ms 3-phase fault in the middle of one of the 220 km transmission lines is experimented. Two breakers—each in both ends of the line—open 100 ms after the fault, remaining opened until the end of each simulation.
2. Change in active power reference (small-signal analysis)—a 4% step in the active power reference is tested. In this simulation, the power system may present a similar dynamic behaviour of a load decrease.
3. Change in reactive power reference (small-signal analysis)—a -0.1 step in the reactive power reference is set.
4. Sweep of active power reference (frequency response, small signal analysis)—a chirp signal with $\pm 5\%$ of the rated active power is applied. The frequency varies from 1 Hz to 100 Hz within 600 s. The aim of this simulation is to determine the oscillation modes of the power system when it is penetrated by RES compared to the original case (four SGs).
5. Probability density function (PDF) of frequency (statistical analysis)—the variation in grid frequency is analysed for each penetration case.
6. Wind variation (statistical analysis)—30 s Monte Carlo simulation considering a normally distributed pseudorandom wind variation of ± 2 m/s around its rated value. Changes in wind speed occur as gusts each 3 s.

By the end of this paper, the expectation is to gain a deep understanding of the system dynamics under different stability conditions for eight RES penetrations. The next section exploits the simulations results and WTG model cited herein.

3. Results

This section presents the simulation results obtained with eight different cases using time and frequency simulations, according to Section 2. All discussions concerning the results are presented in Section 4.

3.1. Short-Circuit

Figures 7–9 show the behaviour of the active powers, frequencies, and terminal voltages for the eight simulated cases, from (a) to (h), respectively. For all simulations, (a) represents the nominal case with four SGs, (b) has machine 1 as WTG (24% of RES), (c) has machine 3 as WTG (24% of RES), (d) has machine 4 as WTG (24% of RES), (e) has area 2 with WTGs (48% of RES), (f) has machines 1 and 3 as WTGs (48% of RES), (g) has machines 1 and 4 as WTGs (48% of RES), and (h) has machines 1, 3, and 4 as WTGs (72% of RES).

In Figure 7, the internal zoom of each graph highlights the behaviour of each machine during the fault. It is important to remark that the fault takes 200 ms to be cleared; however, the breakers open the faulted transmission line after 100 ms.

Notice that, despite slight transient differences, in cases (b), (c), and (d) (24% of RES), the machines present similar results. In the same manner, cases (f) and (g) also present similar results. For these reasons, Sections 3.2–3.4 consider only the results for the nominal case (a) (0% of RES), WTG in machine 1 case (b) (24% of RES), WTGs in machines 3 and 4 case (e) (48% of RES), and WTGs in machines 1, 3, and 4 in case (h) (72% of RES).

As a complement to Figure 8, Table 1 details the results for RoCoF, percentage of frequency variation, and frequency nadir for each machine (M 1–M 4) for the eight cases.

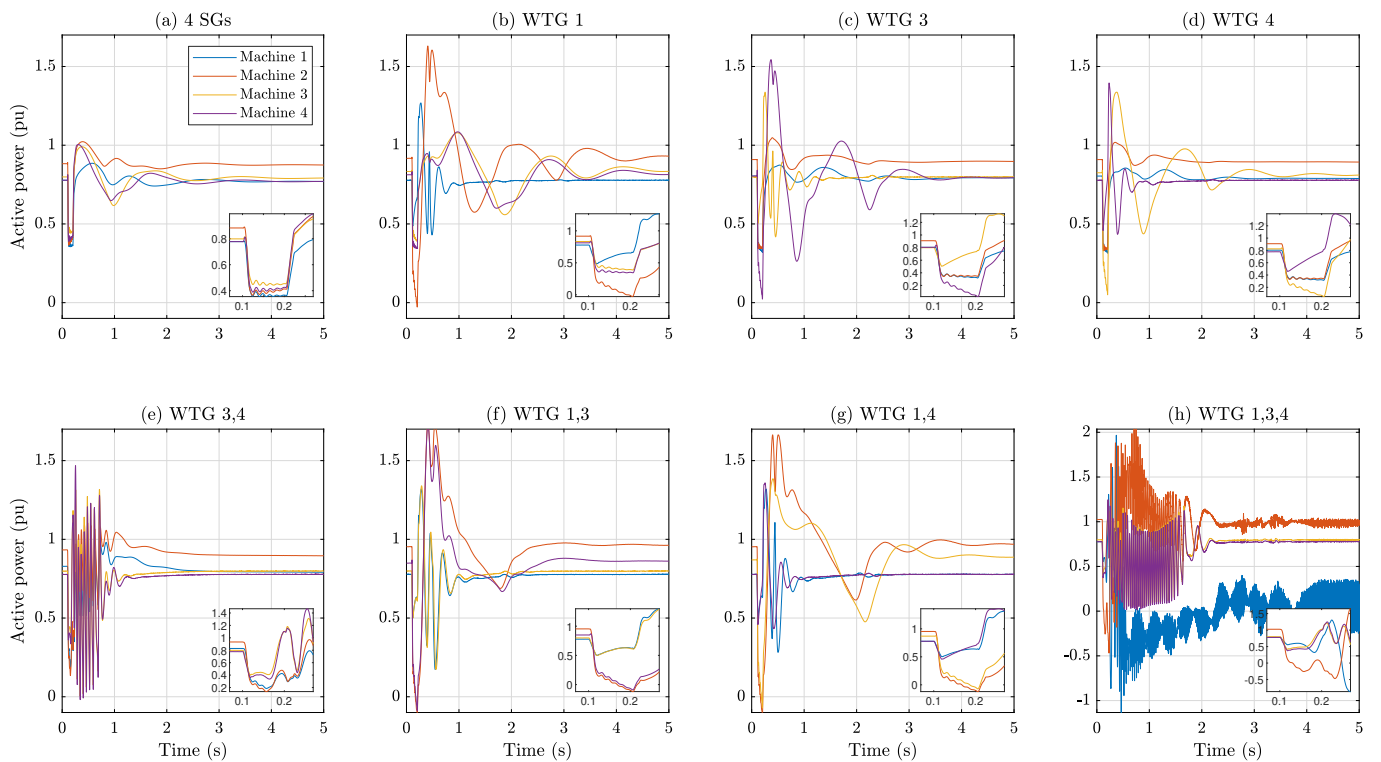


Figure 7. Dynamic behaviour of the active power of the four machines for a 3-phase short-circuit between busbars 7 and 9.

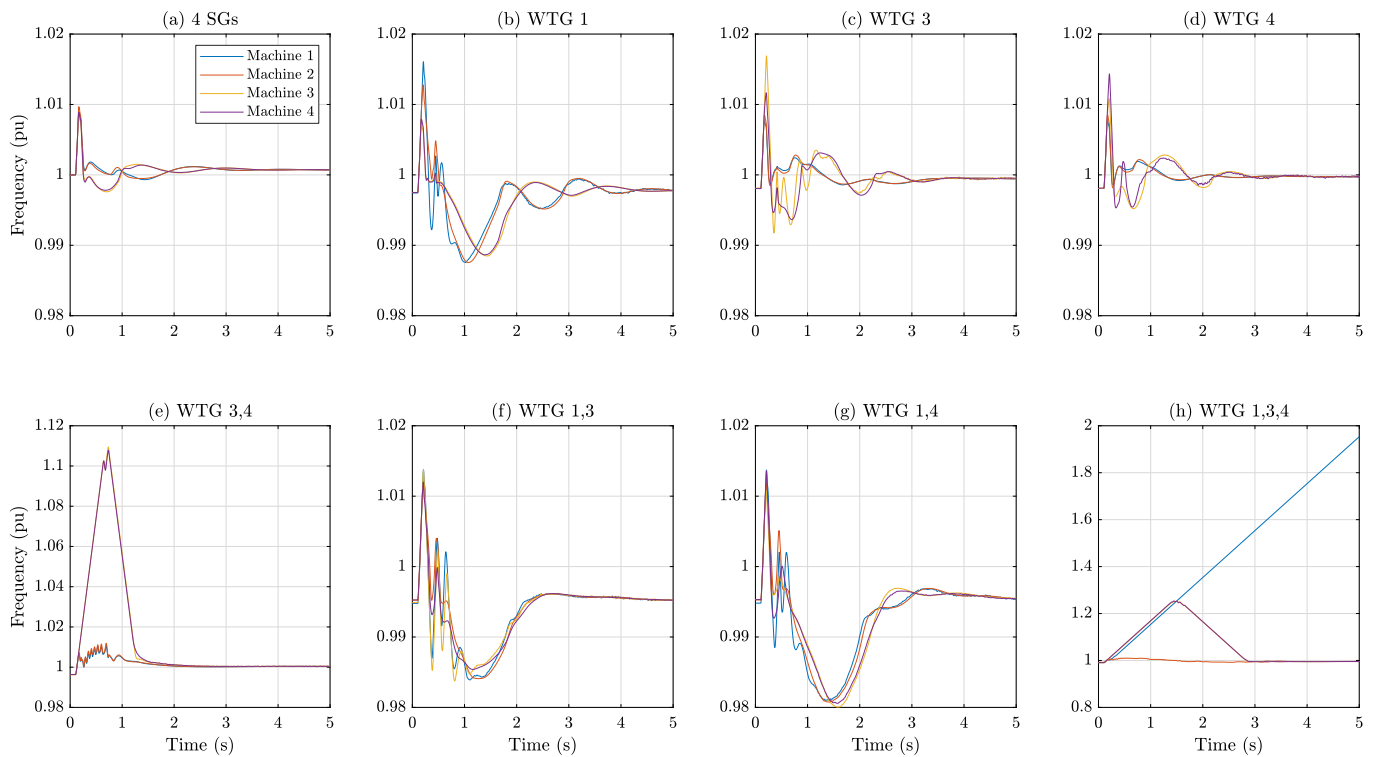


Figure 8. Dynamic behaviour of the frequency of the four machines for a 3-phase short-circuit between busbars 7 and 9.

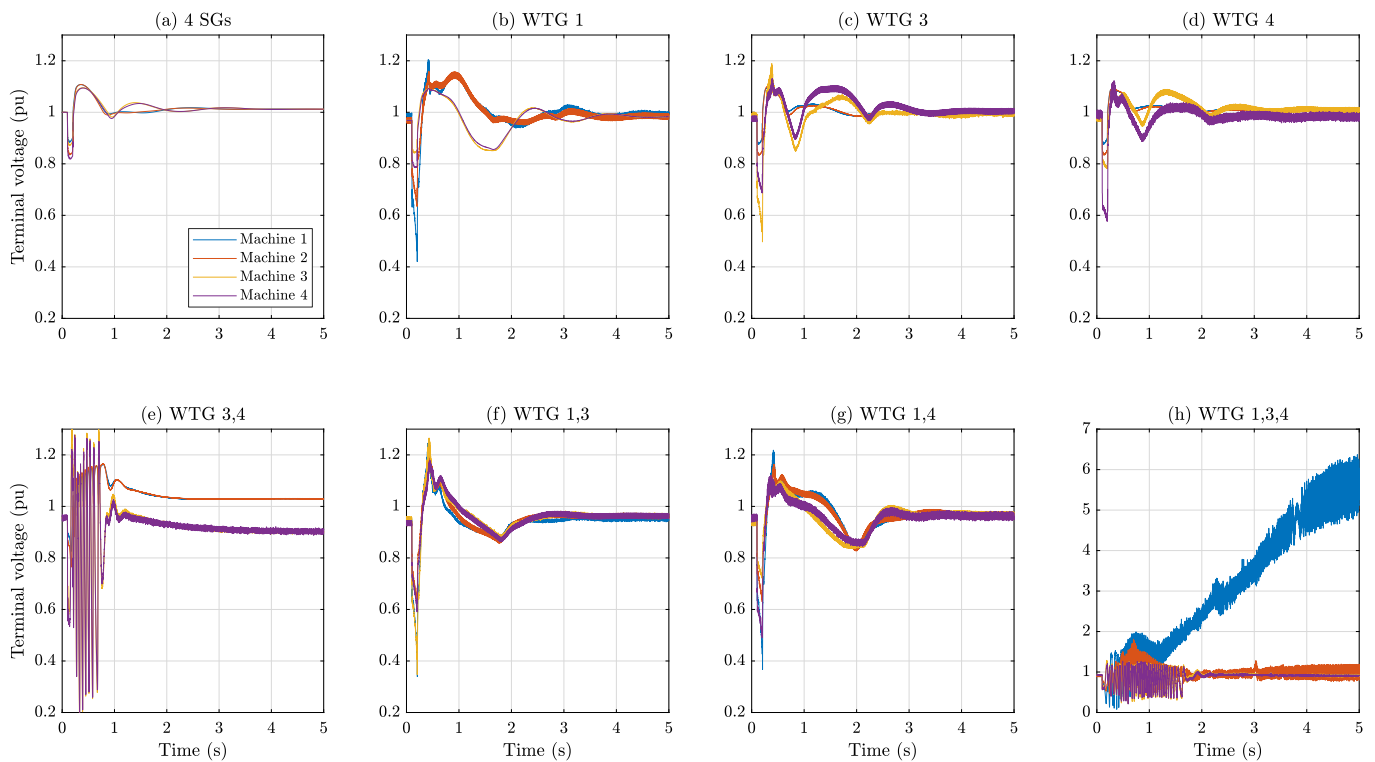


Figure 9. Dynamic behaviour of the terminal voltage of the four machines for a 3-phase short-circuit between busbars 7 and 9.

Table 1. Rate of change of frequency (RoCoF), percentage of frequency variation, and frequency nadir for the short-circuit simulation.

Case	RoCoF (Hz/s)				% of Frequency Variation				Frequency Nadir (Hz)			
	M 1	M 2	M 3	M 4	M 1	M 2	M 3	M 4	M 1	M 2	M 3	M 4
(a)	0.2174	0.2172	0.2171	0.2047	0.90%	0.97%	0.83%	0.89%	0.9946	0.9951	0.9965	0.9972
(b)	0.2071	0.2029	0.1985	0.2033	1.86%	1.53%	0.96%	1.04%	0.9876	0.9875	0.9885	0.9886
(c)	0.1998	0.2027	0.1960	0.2012	0.97%	1.05%	1.28%	1.62%	0.9981	0.9981	0.9952	0.9953
(d)	0.1997	0.2027	0.2039	0.1994	0.96%	1.04%	1.88%	1.36%	0.9981	0.9981	0.9917	0.9936
(e)	0.2175	0.2174	0.2179	0.2178	1.43%	1.55%	11.31%	11.14%	0.9963	0.9963	0.9962	0.9964
(f)	0.2069	0.2033	0.2068	0.2024	1.90%	1.68%	1.88%	1.67%	0.9839	0.9841	0.9838	0.9806
(g)	0.2166	0.2026	0.2014	0.2021	1.89%	1.66%	1.54%	1.83%	0.9810	0.9808	0.9800	0.9806
(h)	0.2145	0.2169	0.2171	0.2172	–	–	–	–	0.9902	0.9900	0.9846	0.9854

3.2. Change in Active Power Reference

Figure 10 shows the results for a 4% step in the active power reference. For cases (a) (0% of RES), (b) (24% of RES), and (d) (72% of RES), the step is applied in machine 1. For case (c) (48% of RES), it is applied in machine 3.

Notice that two results appear for each case, both being presented in column form. For instance, case (a) regards the active power (upper graph) and frequency (bottom graph) variations. The same holds for the remaining cases.

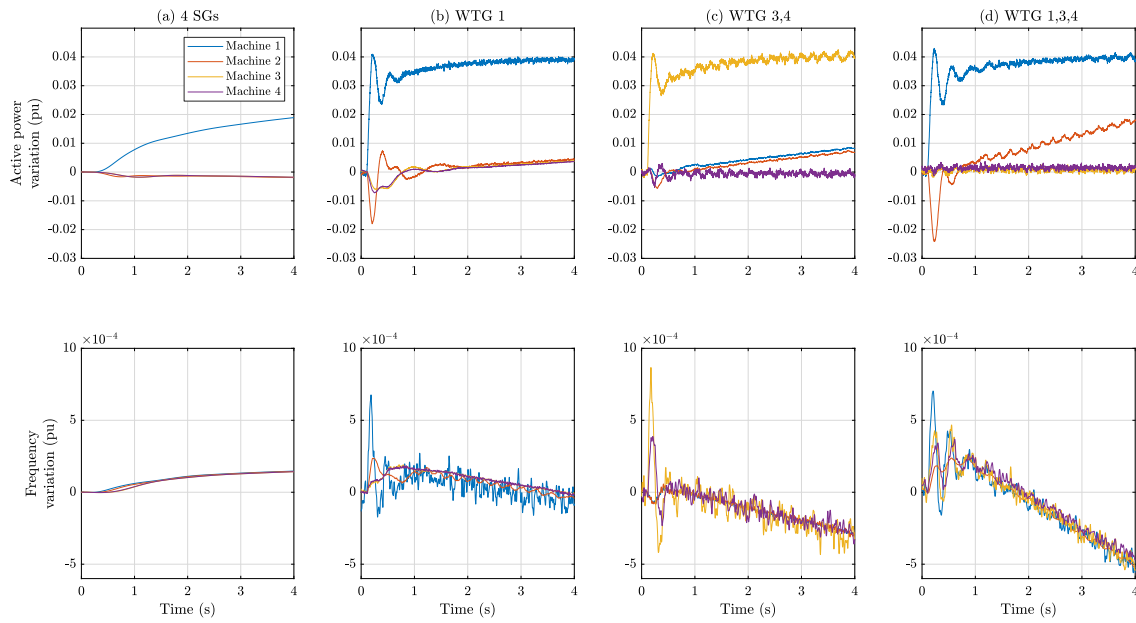


Figure 10. Dynamic behaviour of the active power of the four machines for a 4% step in active power reference.

3.3. Change in Reactive Power Reference

The results for a -0.1 pu step in the reactive power references are presented in Figure 11. As well as in the previous section, cases (a) (0% of RES), (b) (24% of RES), and (d) (72% of RES) have the step applied to machine 1. For case (c) (48% of RES), it is applied in machine 3. Here, the columns represent the reactive power (upper graph) and terminal voltage (bottom graph) of each simulated case.

However, it is important to remark that the SGs used in this work do not have the possibility of reactive power control. Instead, they present the option for terminal voltage control. Therefore, aiming at fair comparisons, in case (a), a step in terminal voltage is used that provides nearly -0.1 pu as well.

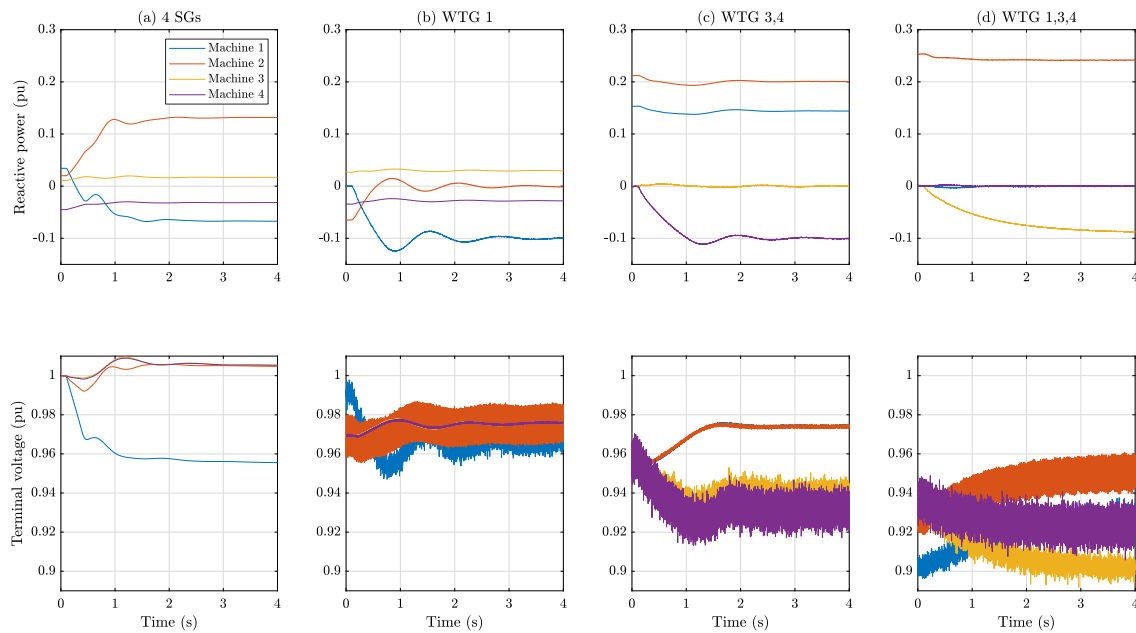


Figure 11. Dynamic behaviour of the reactive power of the four machines for -0.1 pu step in reactive power reference.

3.4. Sweep of Active Power Reference

The power spectral densities (PSDs) for the cases with four SGs (a) (0% of RES), with WTG in machine 1 (b) (24% of RES), with WTGs in machines 3 and 4 (48% of RES), and with WTGs in machines 1, 3, and 4 (d) (72% of RES) are presented in Figure 12. Cases (a) and (b) regard the input signal (chirp) applied in machine 1, whilst cases (c) and (d) concern the application of the chirp signal in machine 4.

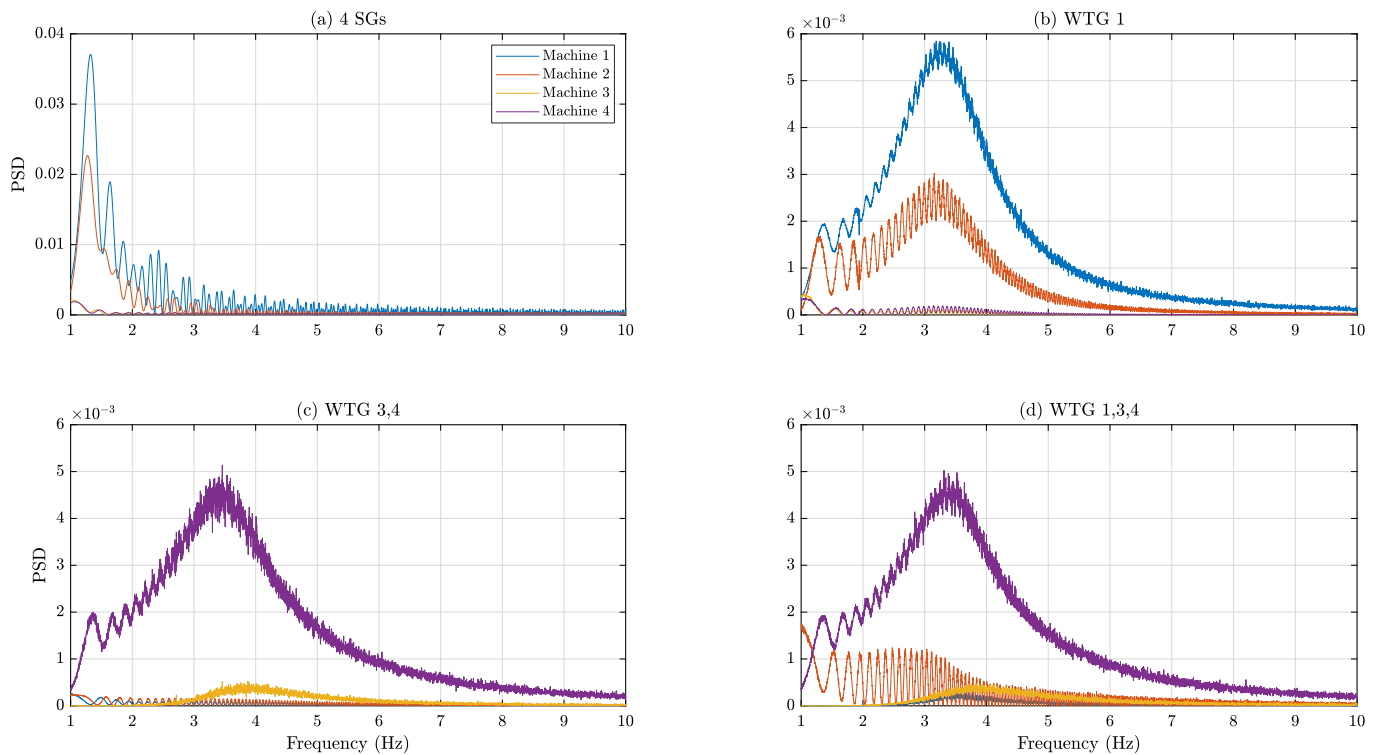


Figure 12. Power spectral densities for the four machines with different RES penetrations.

3.5. PDF of Frequency

The probability density functions (PDFs) for the eight original cases are presented in Figure 13, where case (a) represents the nominal one (0% of RES), case (b) regards machine 1 as WTG (24% of RES), case (c) concerns machine 3 as WTG (24% of RES), in case (d) machine 4 is a WTG (24% of RES), case (e) shows area 2 with WTGs (48% of RES), case (f) presents machines 1 and 3 as WTGs (48% of RES), case (g) regards machines 1 and 4 as WTGs (48% of RES), and machines 1, 3, and 4 are concerned WTGs in case (h) (72% of RES). The frequencies are measured at the machines' terminals.

3.6. Wind Variation

The last results presented in Figure 14 show the system response to wind variation introduced by the Monte Carlo simulations. Here, case (a) concerns machine 1 as WTG (24% of RES), case (b) regards machines 3 and 4 as WTGs (48% of RES), and case (c) shows the results for machines 1, 3, and 4 as WTGs (72% of RES). As well as for previous simulations, each case is presented in column form with results for the active powers (upper graphs) and frequencies (bottom graphs).

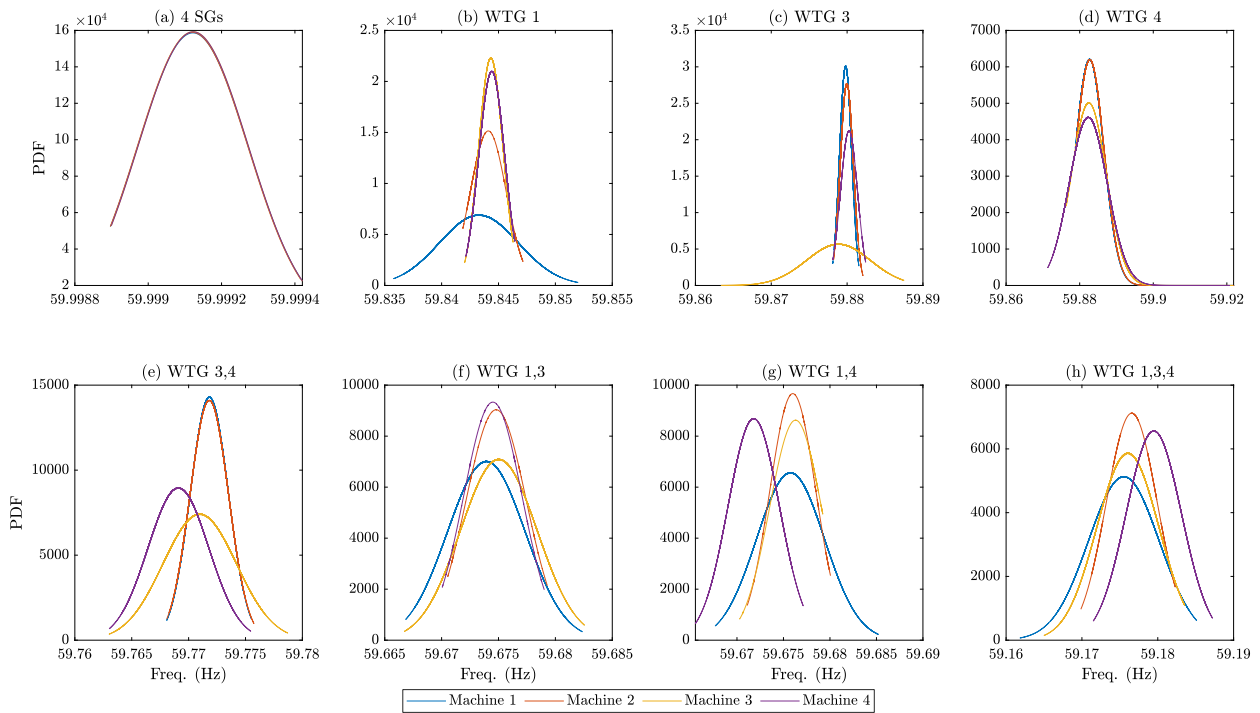


Figure 13. Probability density function (PDF) for the eight study cases.

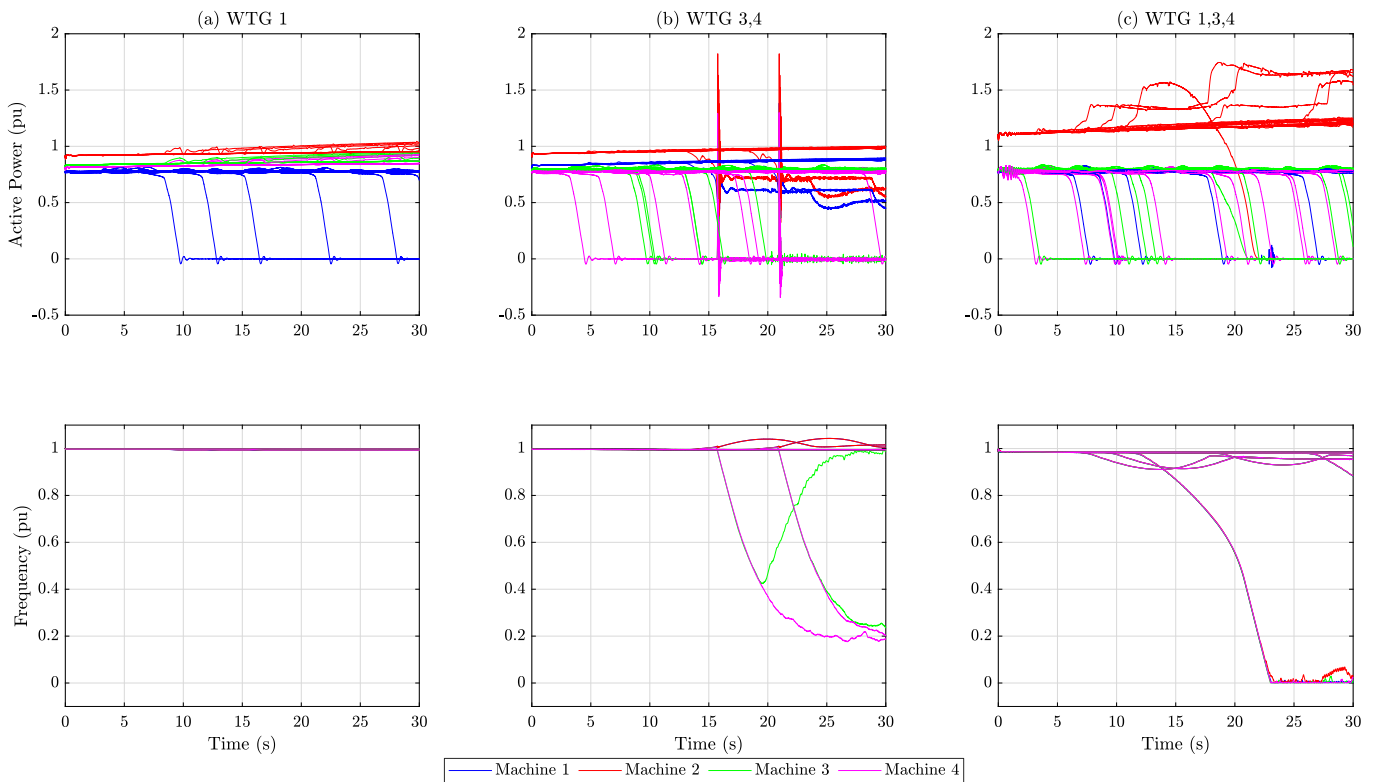


Figure 14. Monte Carlo simulations for the three main study cases: upper figures show the active power of the four machines, whilst bottom figures show the behaviour of their frequencies.

4. Discussion

This section provides an in-depth analysis and interpretation of the results presented in Section 3, organised into separate subsections corresponding to each simulation outcome.

4.1. Short-Circuit

In comparison with the nominal case (Figure 7a), it is noticed that the insertion of WTG in the system changes its transient behaviour.

Cases (b), (c), and (d) show that the machine that is replaced by a WTG (machines 1, 3, and 4, respectively) present similar oscillation behaviour, with maximum amplitude around 1.3 pu, recovering from the fault in less than 1 s. These three cases also present interesting behaviour for their closest SG (machines 2, 4, and 3, respectively): for each separated case, these machine are the ones that presented both the higher oscillation amplitudes and longer time to reach the steady state. In case (b), it is also possible to observe a clear interarea oscillation between generating areas 1 and 2, mainly wrt machine 2 against machines 3 and 4. This behaviour is not observed in cases (c) and (d), which represent the same penetration ratio as in case (b). These results are aligned with numerous studies in the literature that emphasise the significance of the WTG location as a crucial parameter in power system design.

Case (e) shows the instability created after the fault, with area 2 being fully composed of WTGs. Notice that all machines oscillate abruptly for more than 0.5 s. Despite returning relatively fast to steady state, the oscillatory behaviour indicates that the power system is close to instability, and countermeasures might be applied.

Cases (f) and (g) present very similar results, with case (g) showing slightly more oscillations than in case (f). Both cases represent the most symmetric representation of the power system, with one WTG in each generating area (48% of RES). Again, the WTGs present fewer oscillations than the SGs. However, it is noticeable that their oscillations demonstrate strong nonlinear behaviour, different from the oscillations presented in cases (b)–(d), where the system has 24% of RES penetration.

Finally, case (h) shows that the power system, in the way it is designed in this paper, is not able to maintain synchronism after a fault when penetrated by 72% of RES; in this case, machines 1, 3, and 4 are WTGs.

Figures 8 and 9 complement the results discussed from Figure 7.

In Figure 8, it is also observed that the nominal case (a) presents less post-fault frequency oscillations than any other. Cases (b), (f), and (g) show frequency variations that would fit into the category of “tolerable abnormal operating range” [40]. In cases (c) and (d), this variation is within the operating range. However, case (e) (area 2 fully RES) presents a frequency variation for machines 3 and 4 that extrapolates the operating limits of the power system. Again, case (h) shows a loss in synchronism that would lead to a global blackout.

Table 1 complements the results of Figure 8. It is interesting to notice that the highest RoCoF values occur for cases (a), (e), and (h). The smallest RoCoF values are present in cases (c) and (d). Despite this, it is important to highlight that the WTGs do not significantly alter the RoCoF values of the system.

The same table still shows the frequency nadir and the percentage of frequency variation. It is decided to show both amounts since the frequency nadir does not always represent the best measure to understand the variation in the frequency signals. For instance, it is observed that the lowest frequency nadir happens for case (g). However, according to the results presented in Figure 8, case (e) shows a very high positive frequency variation after the fault. Table 1 informs that the percentage of the frequency variation in this case is above 11% for machines 3 and 4. In practice, these variations would activate protection systems to ensure the grid stability.

Notice that, apart from case (e) and case (h)—where there is a loss in synchronism—the frequency variations remain below 2% for all cases.

The behaviour of the terminal voltages is shown in Figure 9. The voltage drop is slightly greater than 10% after the fault for cases (b), (c), (d), (f), and (g). In comparison to the nominal case (a), these five cases also present a higher voltage drop during the fault. Notice also that cases (e), (f), and (g) present steady state values lower than 1 pu for the terminal voltages. In case (e) (area 2 fully RES), voltage steady state is 0.9 pu in area 2,

which is below the operating limits of the power system. Cases (f) and (g) (48% of RES) present nearly 0.95 pu for the steady state value of the terminal voltages. Again, case (h) shows that there is a loss in synchronism in the power system after the fault.

It is important to acknowledge the terminal voltage profiles of WTGs as they exhibit higher levels of noise compared to SGs. This outcome is to be expected in practical scenarios due to the inverter switchings. However, it is worth noting that this aspect is not always adequately addressed in the literature, primarily due to simplifications and the use of average models.

4.2. Change in Active Power Reference

Figure 10 shows the simulation results for the four main cases, namely: (a) with four SGs (0% of RES), (b) with machine 1 as WTG (24% of RES), (c) with area 2 fully RES (48% of RES), and (d) with machines 1, 3, and 4 as WTGs (72% of RES). This simulation experiments system small-signal stability.

All the graphs show the results until 4 s. However, this time frame is only used to better show the details of the power step for each case. Therefore, it is important to remark that, for all cases, power and frequency steady state values are only reached in longer periods. For instance, in the nominal case (a), the new active power reference is only reached after nearly 10 s.

In comparison, the WTGs in cases (b), (c), and (d) are able to reach the active power reference within 4 s in a very stable manner. However, the sharp increase in their active powers reflects in oscillations in the SG machines. As an example, in case (b), the SGs oscillate oppositely to the step in active power of the WTG, presenting also a very slow oscillation that damps out after nearly 25 s. The same behaviour is noticed in cases (c) and (d), with increasing oscillation amplitude whenever the RES penetration increases.

Similarly, it is also noticed that the frequency drops are steeper with the increase in RES penetration, reflecting also the increase in active power delivered by the machines. Worth noting as well is the noise in the WTGs frequency in comparison with SGs.

4.3. Change in Reactive Power Reference

In Figure 11, a 0.1 pu drop in reactive power is experienced for the same four cases presented in Section 4.2.

An expected result that can be clearly observed in the results is that the SGs reactive powers compensate for the lack of reactive powers of the WTGs since the latter have reactive power references equal to zero. Hence, the higher the RES penetration, the higher the reactive power of the remaining SGs in the system.

It is also remarkable that the oscillations in reactive power after the step are more pronounced for systems with less RES penetration, as in case (b).

Concerning the behaviour of the terminal voltages, it is observed that the increase in RES penetration impacts negatively the terminal voltage steady state value. Case (c) presents terminal voltage values for machines 3 and 4 (both WTGs) that are outside the operating limits, whilst the same limits are transgressed by machines 1, 3, and 4 (all WTGs) in case (d).

4.4. Sweep of Active Power Reference

The experiment presented in Figure 12 also highlights the small-signal stability but aiming at the possible oscillation modes presented in the system.

It is observed in case (a) that the nominal system has a very pronounced oscillation mode around 1.3 Hz, which is known in the literature as being an interarea mode.

Notably, none of the tested systems (with RES penetration levels of 24%, 48%, and 72% in cases (b), (c), and (d), respectively) exhibited a significant interarea mode. The findings indicate that the 1.3 Hz oscillation mode is effectively damped in all cases, with the highest mode now occurring at approximately 3.2 Hz. However, it is worth mentioning that, although the oscillation bandwidth has increased, the amplitude of this mode is

significantly lower compared to the nominal case. Consequently, the power system is not adversely affected to the same extent as it is by the 1.3 Hz oscillation.

A deeper investigation is carried out to understand why there is no important interarea mode whenever WTGs are inserted in the tested power system. The interarea modes are characterised by low frequency oscillations caused mainly by large power exchanges between two or more generating areas. These modes are inherently tied to the system synchronous inertia.

Therefore, the increase in RES penetration operates in two fronts: first by reducing the total synchronous inertia of the system, which causes eventual modes to have higher frequencies, and second by the ordinary implementation of WTG controllers, which inherently damps out the low-frequency modes presented in the system. This is mainly completed by the active power controller, but not only by it. Less inertia means that the integral times of the PI controllers can be tuned using lower values, which increases the bandwidth, helping in filtering out lower frequencies.

4.5. PDF of Frequency

Figure 13 details a result that was shortly explored in Section 4.2, which is the frequency deviation and noise wrt of the penetration of RES in the tested power system, analysing now their probability density functions (PDFs).

The increase in RES impacts negatively the frequency steady state value. Notice that cases (b), (c), and (d) (all with 24% of RES) present nearly the same frequency for the SGs, which is greater than 59.84 Hz for all three. Cases (b) and (c) present similar results, with the WTG showing a spread PDF in comparison with the SGs. Remarkably, this fact does not occur in case (d), where all machines have similar PDF profiles. On the other hand, for the cases with 48% of RES penetration (cases (e), (f), and (g)), there is a frequency drop to around 59.7 Hz, with a more pronounced PDF spread of the WTGs. Lastly, case (h) shows that the frequency mean value is around 59.18 Hz for 72% of RES penetration, which is clearly dangerous for the power system integrity.

4.6. Wind Variation

The Monte Carlo simulation results shown in Figure 14 detail the behaviour of the power system for pseudo-random wind variations.

Case (a) (machine 1 as WTG) shows that, among thirty simulations with ten wind variations each, for five times, there is a loss in synchronism in the WTG, representing 1.67% of all wind variations. However, the remaining grid—which is composed of SGs—is capable of compensating the lack of generation of machine 1. The frequency oscillates and returns to its steady state.

In case (b) (machines 3 and 4 as WTGs), the same amount of simulations have shown that machine 3 has lost its synchronism for six times, whilst the same happened for machine 4 for seven times, which represents 4.33% of the tested systems. There was never a simultaneous loss in synchronization for machines 3 and 4. In all cases, the remaining grid was capable of keeping the system stability. For two times, there are steep frequency drops, which are fully recovered after 30 s. In practice, these drops would lead to the trip of all machines in area 2.

Finally, case (c) (machines 1, 3, and 4 as WTGs) shows that there is loss in synchronism for twenty-six times (8.67% of the tested cases): five times for machine 1, nine times for machine 3, ten times for machine 4, and once for machine 2 (swing bus). The loss in synchronism of machine 2 is the cause for the grid collapse observed in the frequency graph in case (c). Despite some oscillations, all machines recover their frequency levels for the other cases.

5. Conclusions

This work provides a comprehensive analysis of the impact of RES penetration on an IEEE benchmark system. The study utilises detailed type 4 WTG, which include various

components, such as wind turbines, generators, rectifiers, boost converters, inverters, and filters. The controllers employed include pitch control, active and reactive power control, DC-link control, and field voltage control. Eight different scenarios are simulated, ranging from 0% to 72% RES penetration. The analysis focuses on transient and small-signal stability, as well as statistical analysis, to shed light on the complex dynamics of modern power systems.

The transient stability study, conducted through short-circuit analysis, reveals that the introduction of RES into the two-area benchmark system significantly alters its oscillatory behaviour compared to the nominal case with four SGs. A 24% RES penetration primarily impacts the amplitude and oscillation duration following a fault. However, a 48% penetration indicates that the power system begins to exhibit stability issues. For instance, frequency and voltage limits are exceeded when area 2 relies solely on RES. Finally, the system experiences complete loss in synchronism at 72% RES penetration, suggesting that, for the simulated power transfer amount, the power system becomes unstable.

In general, the results demonstrate that increased RES penetration negatively affects the system frequency, ranging from 60 Hz with 0% RES to 59.18 Hz with 72% RES. This variation is significant because the normal operation limit for the system is 59.5 Hz, which is maintained up to 48% RES penetration.

Additionally, the paper reveals that wind speed variations of ± 2 m/s around the rated value of the wind turbine generator can impact active power transfer. Despite this, power systems with 24% and 48% RES penetration are still capable of maintaining stability, whereas the simulation indicates a collapse of the entire power system at 72% RES penetration.

An interesting finding pertains to the interarea mode as the common 1.3 Hz oscillations do not occur in the system with RES penetration due to the presence of inherent controllers in the WTG.

One of the major challenges encountered in this study was the simulation time. Given the numerous simulations conducted, a substantial amount of time was required to complete them all. Future research should consider using real-time simulation systems to overcome this limitation. Moreover, further experiments should be conducted to analyse RES penetration ranging from 0% to 50% in order to study the system within its stability limits. Additionally, it would be interesting to replace the WTGs with solar PV and battery cells to investigate their dynamic behaviours within the same IEEE benchmark system.

Author Contributions: Conceptualisation, R.T. and R.K.; methodology, R.T.; software, R.T. and J.J.A.S.; validation, R.T., J.J.A.S. and A.N.; formal analysis, R.K. and A.N.; investigation, R.T.; resources, R.T.; data curation, A.N.; writing—original draft preparation, R.T.; writing—review and editing, R.T., R.K., J.J.A.S., A.N., T.J.M.D. and M.S.M.C.; visualisation, R.T.; supervision, R.K. and A.N.; project administration, R.K.; funding acquisition, A.N., T.J.M.D. and M.S.M.C. All authors have read and agreed to the published version of the manuscript.

Funding: This research received no external funding. The APC was funded by the Fundação de Amparo à Pesquisa e Inovação do Estado de Santa Catarina: Termo de Outorga 2021TR999.

Data Availability Statement: The data presented in this study are available on request from the corresponding author. The data are not publicly available due to the lack of an institutional repository.

Conflicts of Interest: The authors declare no conflict of interest.

References

1. International Energy Agency (IEA). *World Energy Outlook 2022*; IEA: Paris, France, 2022.
2. International Energy Agency (IEA). *Wind Electricity*; IEA: Paris, France, 2022.
3. Padrón, S.; Hernández, M.; Falcón, A. Reducing under-frequency load shedding in isolated power systems using neural networks. Gran Canaria: A case study. *IEEE Trans. Power Syst.* **2015**, *31*, 63–71. [[CrossRef](#)]
4. Shair, J.; Li, H.; Hu, J.; Xie, X. Power system stability issues, classifications and research prospects in the context of high-penetration of renewables and power electronics. *Renew. Sustain. Energy Rev.* **2021**, *145*, 111111. [[CrossRef](#)]

5. Ratnam, K.S.; Palanisamy, K.; Yang, G. Future low-inertia power systems: Requirements, issues, and solutions—A review. *Renew. Sustain. Energy Rev.* **2020**, *124*, 109773. [[CrossRef](#)]
6. Ferreira, Y.R.; Trentini, R.; Kutzner, R. Control strategy for Inertia Emulation through Grid-Following Inverters. In Proceedings of the 2021 9th International Conference on Systems and Control (ICSC), Caen, France, 24–26 November 2021.
7. Elnaggar, A.; Rueda, J.; Erlich, I. Comparison of short-circuit current contribution of Doubly-Fed induction generator based wind turbines and synchronous generator. In Proceedings of the 2013 IEEE Grenoble Conference, Dresden, Germany, 26–27 September 2013.
8. Wu, T.; Xie, X.; Jiang, Q.; Shen, Z. Impedance modelling of grid-connected voltage-source converters considering the saturation non-linearity. *IET Gener. Transm. Distrib.* **2020**, *14*, 4815–4823. [[CrossRef](#)]
9. Shah, S.; Koralewicz, P.; Gevorgian, V.; Wallen, R.; Jha, K.; Mashtare, D.; Burra, R.; Parsa, L. Large-signal impedance-based modeling and mitigation of resonance of converter-grid systems. *IEEE Trans. Sustain. Energy* **2019**, *10*, 1439–1449. [[CrossRef](#)]
10. Mansour, M.Z.; Me, S.P.; Hadavi, S.; Badrzadeh, B.; Karimi, A.; Bahrani, B. Nonlinear transient stability analysis of phased-locked loop-based grid-following voltage-source converters using Lyapunov's direct method. *IEEE J. Emerg. Sel. Top. Power Electron.* **2021**, *10*, 2699–2709. [[CrossRef](#)]
11. Saha, S.; Saleem, M.; Roy, T. Impact of high penetration of renewable energy sources on grid frequency behaviour. *Int. J. Electr. Power Energy Syst.* **2023**, *145*, 108701. [[CrossRef](#)]
12. Alam, M.; Chowdhury, T.A.; Dhar, A.; Al-Ismail, F.S.; Choudhury, M.; Shafiullah, M.; Hossain, M.; Ullah, A.; Rahman, S.M. Solar and Wind Energy Integrated System Frequency Control: A Critical Review on Recent Developments. *Energies* **2023**, *16*, 812. [[CrossRef](#)]
13. Obradović, D.; Dijokas, M.; Misyris, G.S.; Weckesser, T.; Van Cutsem, T. Frequency dynamics of the Northern European AC/DC power system: A look-ahead study. *IEEE Trans. Power Syst.* **2022**, *37*, 4661–4672. [[CrossRef](#)]
14. Fernández-Guillamón, A.; Gómez-Lázaro, E.; Muljadi, E.; Molina-García, Á. Power systems with high renewable energy sources: A review of inertia and frequency control strategies over time. *Renew. Sustain. Energy Rev.* **2019**, *115*, 109369. [[CrossRef](#)]
15. Yi, W.; Hill, D.J.; Song, Y. Impact of high penetration of renewable resources on power system transient stability. In Proceedings of the 2019 IEEE Power & Energy Society General Meeting (PESGM), Atlanta, GA, USA, 4–8 August 2019.
16. Shair, J.; Xie, X.; Liu, W.; Li, X.; Li, H. Modeling and stability analysis methods for investigating subsynchronous control interaction in large-scale wind power systems. *Renew. Sustain. Energy Rev.* **2021**, *135*, 110420. [[CrossRef](#)]
17. Flynn, D.; Rather, Z.; Årdal, A.R.; D'Arco, S.; Hansen, A.D.; Cutululis, N.A.; Sorensen, P.; Estante, A.; Gómez-Lázaro, E.; Menemenlis, N.; et al. Technical impacts of high penetration levels of wind power on power system stability. In *Advances in Energy Systems: The Large-scale Renewable Energy Integration Challenge*; John Wiley & Sons: Hoboken, NJ, USA, 2019.
18. Knüppel, T.; Nielsen, J.N.; Jensen, K.H.; Dixon, A.; Østergaard, J. Small-signal stability of wind power system with full-load converter interfaced wind turbines. *IET Renew. Power Gener.* **2012**, *6*, 79–91. [[CrossRef](#)]
19. Du, W.; Bi, J.; Wang, T.; Wang, H. Impact of grid connection of large-scale wind farms on power system small-signal angular stability. *CSEE J. Power Energy Syst.* **2015**, *1*, 83–89. [[CrossRef](#)]
20. Baquedano-Aguilar, M.; Colomé, D.; Agüero, E.; Molina, M. Impact of increased penetration of large-scale PV generation on short-term stability of power systems. In Proceedings of the 2016 IEEE 36th Central American and Panama Convention (CONCAPAN XXXVI), San Jose, Costa Rica, 9–11 November 2016.
21. Tróndheim, H.M.; Hofmann, L.; Gartmann, P.; Quitmann, E.; Bak, C.L.; da Silva, F.M.F.; Nielsen, T.; Niclasen, B.A. Frequency and Voltage Stability towards 100% Renewables in Suðuroy, Faroe Islands. *CIGRE Sci. Eng.* **2022**. Available online: <https://cse.cigre.org/cse-n025/frequency-and-voltage-stability-towards-100-renewables-in-suduroy-faroe-islands> (accessed on 16 May 2023).
22. Taul, M.G.; Wang, X.; Davari, P.; Blaabjerg, F. Systematic approach for transient stability evaluation of grid-tied converters during power system faults. In Proceedings of the 2019 IEEE Energy Conversion Congress and Exposition (ECCE), Baltimore, MD, USA, 29 September–3 October 2019.
23. Gayathri, K.; Jena, M.K.; Moharana, A.K. Impact of different penetration level of type-iv renewable energy resources on power system dynamics. In Proceedings of the 2021 9th IEEE International Conference on Power Systems (ICPS), Kharagpur, India, 16–18 December 2021.
24. Wilches-Bernal, F.; Lackner, C.; Chow, J.H.; Sanchez-Gasca, J.J. Effects of wind turbine generators on inter-area oscillations and damping control design. In Proceedings of the 2019 52nd Hawaii International Conference on System Sciences, Maui, HI, USA, 8–11 January 2019.
25. Piccoli, D.C.; Trentini, R.; Saldanha, J.J.A. Synchronous Inertia Deficit: A Study on Electric Power Systems with High Penetration of Renewable Energy Sources. In Proceedings of the 2021 9th International Conference on Systems and Control (ICSC), Caen, France, 24–26 November 2021.
26. Tong, N.; Jiang, Z.; You, S.; Zhu, L.; Deng, X.; Xue, Y.; Liu, Y. Dynamic equivalence of large-scale power systems based on boundary measurements. In Proceedings of the 2020 American Control Conference (ACC), Denver, CO, USA, 1–3 July 2020.
27. Dong, W.; Xin, H.; Wu, D.; Huang, L. Small signal stability analysis of multi-infeed power electronic systems based on grid strength assessment. *IEEE Trans. Power Syst.* **2018**, *34*, 1393–1403. [[CrossRef](#)]
28. Ochoa, D.; Martinez, S.; Arévalo, P. Extended Simplified Electro-Mechanical Model of a Variable-Speed Wind Turbine for Grid Integration Studies: Emulation and Validation on a Microgrid Lab. *Electronics* **2022**, *11*, 3945. [[CrossRef](#)]

29. Chou, S.F.; Wang, X.; Blaabjerg, F. Two-port network modeling and stability analysis of grid-connected current-controlled VSCs. *IEEE Trans. Power Electron.* **2019**, *35*, 3519–3529. [[CrossRef](#)]
30. Fan, L. Modeling type-4 wind in weak grids. *IEEE Trans. Sustain. Energy* **2018**, *10*, 853–864. [[CrossRef](#)]
31. Beza, M.; Bongiorno, M. On the risk for subsynchronous control interaction in type 4 based wind farms. *IEEE Trans. Sustain. Energy* **2018**, *10*, 1410–1418. [[CrossRef](#)]
32. O’Sullivan, J.; Rogers, A.; Flynn, D.; Smith, P.; Mullane, A.; O’Malley, M. Studying the maximum instantaneous non-synchronous generation in an island system—Frequency stability challenges in Ireland. *IEEE Trans. Power Syst.* **2014**, *29*, 2943–2951. [[CrossRef](#)]
33. Wang, Y.; Delille, G.; Bayem, H.; Guillaud, X.; Francois, B. High wind power penetration in isolated power systems—Assessment of wind inertial and primary frequency responses. *IEEE Trans. Power Syst.* **2013**, *28*, 2412–2420. [[CrossRef](#)]
34. Kundur, P.; Klein, M.; Rogers, G.; Zywno, M.S. Application of power system stabilizers for enhancement of overall system stability. *IEEE Trans. Power Syst.* **1989**, *4*, 614–626. [[CrossRef](#)]
35. Jamal, A.; Syahputra, R. Adaptive Neuro-Fuzzy Approach for the Power System Stabilizer Model in Multi-machine Power System. *Int. J. Electr. Comput. Sci. IJECS* **2012**, *12*. Available online: <https://citeseerx.ist.psu.edu/document?repid=rep1&type=pdf&doi=d498deb226960217c5ce5d340515cbd5c05f189a> (accessed on 16 May 2023).
36. Kundur, P.; Paserba, J.; Ajarapu, V.; Andersson, G.; Bose, A.; Canizares, C.; Hatziargyriou, N.; Hill, D.; Stankovic, A.; Taylor, C.; et al. Definition and classification of power system stability IEEE/CIGRE joint task force on stability terms and definitions. *IEEE Trans. Power Syst.* **2004**, *19*, 1387–1401.
37. Trentini, R. Contributions to the Damping of Interarea Modes in Extended Power Systems: A Turbine Governor Approach with the Help of the Unrestricted Horizon Predictive Controller. Ph.D. Thesis, Gottfried Wilhelm Leibniz Universität Hannover, Hannover, Germany, 2017.
38. Singh, M.; Santoso, S. *Dynamic Models for Wind Turbines and Wind Power Plants*; Technical Report; National Renewable Energy Lab. (NREL): Golden, CO, USA, 2011.
39. Trevisan, A.S.; El-Deib, A.A.; Gagnon, R.; Mahseredjian, J.; Fecteau, M. Field validated generic EMT-type model of a full converter wind turbine based on a gearless externally excited synchronous generator. *IEEE Trans. Power Deliv.* **2018**, *33*, 2284–2293. [[CrossRef](#)]
40. Machowski, J.; Lubosny, Z.; Bialek, J.W.; Bumby, J.R. *Power System Dynamics: Stability and Control*; John Wiley & Sons: Hoboken, NJ, USA, 2020.

Disclaimer/Publisher’s Note: The statements, opinions and data contained in all publications are solely those of the individual author(s) and contributor(s) and not of MDPI and/or the editor(s). MDPI and/or the editor(s) disclaim responsibility for any injury to people or property resulting from any ideas, methods, instructions or products referred to in the content.